HYDROGEN-AIR DEFLAGRATIONS: VENT SIZING CORRELATION FOR LOW-STRENGTH EQUIPEMENT AND BUILDINGS

Molkov, V.[1], and Bragin, M.[2]*
[1] **Hydrogen Safety Engineering and Research Centre (HySAFER), University of Ulster, Shore Road, Newtownabbey, BT37 0QB, Northern Ireland, UK**
[2] **Wolfson School of Mechanical and Manufacturing Engineering, Loughborough University, Epinal Way, Loughborough, LE11 3TU, UK**

Abstract

This paper aims to improve prediction capability of the vent sizing correlation presented in the form of functional dependence of the dimensionless deflagration overpressure on the turbulent Bradley number similar to our previous studies. The correlation is essentially upgraded based on recent advancements in understanding and modelling of combustion phenomena relevant to hydrogen-air vented deflagrations and unique large-scale tests carried out by different research groups. The focus is on hydrogen-air deflagrations in low-strength equipment and buildings when the reduced pressure is accepted to be below 0.1 MPa. The combustion phenomena accounted for by the correlation include: turbulence generated by the flame front itself; leading point mechanism stemming from the preferential diffusion of hydrogen in air in stretched flames; growth of the fractal area of the turbulent flame surface; initial turbulence in the flammable mixture; as well as effects of enclosure aspect ratio and presence of obstacles. The correlation is validated against the widest range of experimental conditions available to date (76 experimental points). The validation covers a wide range of test conditions: different shape enclosures of volume up to 120 m^3; initially quiescent and turbulent hydrogen-air mixtures; hydrogen concentration in air from 6% to 30% by volume; ignition source location at enclosure centre, near and far from a vent; empty enclosures and enclosures with obstacles.

Keywords: Hydrogen, vented deflagration, experimental data, correlation, validation.

Nomenclature

A_{EW}	area of enclosure internal surface (m^2)
A_W	area of the sphere with volume equal to enclosure volume (m^2)
Br	Bradley number
Br_t	turbulent Bradley number
c_{ui}	speed of sound (m/s)
D	fractal dimension
E_i	combustion products expansion coefficient, $E_i = M_{ui}T_{bi}/M_{bi}T_{ui}$
e, g	empirical coefficients in equation (6)
F	vent area (m^2)
M	molecular mass (g/mol)
P_i	initial pressure (Pa abs)
P_{max}	maximum absolute pressure (Pa abs)
P_{red}	reduced pressure (Pa gauge)
P_{stat}	static activation pressure (Pa gauge)
R	flame radius (maximum) (m)
R_u	universal gas constant, 8.31 J/K/mol
R_0	critical radius (m)
S_t	turbulent burning velocity (m/s)
S_{ui}	initial laminar burning velocity (m/s)
T	temperature (K)
V	volume of enclosure (m^3)
$V_\#$	dimensionless volume (numerically equal to enclosure volume in cubic meters)
X	hydrogen mole fraction

Greek

$\alpha,\beta,\delta\omega$	empirical coefficients in equation (6)
γ_u	specific heat ratio
π_0	"Pi" number, 3.141
$\pi_{i\#}$	dimensionless initial pressure (numerically equal to initial pressure in absolute atmospheres)
π_{red}	dimensionless reduced pressure, P_{red}/P_i;
π_v	dimensionless static activation pressure $\pi_v = (P_{stat}+P_i)/P_i$

* Corresponding author. Tel.: +44 1509227684.
E-mail addresses: v.molkov@ulster.ac.uk (V. Molkov), m.bragin@lboro.ac.uk (M. Bragin)

χ/μ deflagration-outflow interaction (DOI) number
ψ empirical coefficient
Ξ_K wrinkling factor due to turbulence generated by the flame front itself
Ξ_K^{max} theoretical maximum of Ξ_K
Ξ_{LP} wrinkling factor due to leading point mechanism
Ξ_{LP}^{max} maximum leading point wrinkling factor
Ξ_{FR} wrinkling factor due to fractal increase of flame surface area
$\Xi_{u'}$ wrinkling factor to account for initial turbulence
Ξ_{AR} wrinkling factor to account for aspect ratio of the enclosure
Ξ_O wrinkling factor to account for the presence of obstacles

Subscripts

b burned mixture
i initial conditions
red reduced
stat static
t turbulent
u unburned mixture

Superscripts

max maximum value

Acronyms

CFD Computational Fluid Dynamics
DOI deflagration-outflow interaction
LES Large Eddy Simulation
SGS sub-grid scale

1. Introduction

Venting of deflagration is the most wide spread technique to reduce overpressure during flammable mixture deflagration indoors or in a system like fuel cells. Different empirical and semi-empirical models were developed and applied for vent sizing of deflagration mitigation systems and published elsewhere. A recent overview of equations for vent sizing and their inter-comparison and comparison against experiments with various hydrocarbon-air and hydrogen-air mixtures can be found in [1].

The vent sizing technique that is advanced further in this study has been under development since 1995 and its developmental progress can be found in publications [2, 3, 4, 5, 6, 8, 9, 10, 11]. The correlation for low-strength equipment and buildings, i.e. when the deflagration overpressure or reduced pressure is below 0.1 MPa (initial pressure in such cases is usually atmospheric equal to 0.1 MPa), is presented by the following equation from our 1999 study [4] that is the best fit to experimental data

$$\pi_{red} = Br_t^{-2.4} \quad (\pi_{red} < 1), \tag{1}$$

where π_{red} is the dimensionless reduced pressure, and Br_t is the turbulent Bradley number

$$Br_t = \frac{\sqrt{E_i / \gamma_u}}{\sqrt[3]{36\pi_0}} \cdot \frac{Br}{\chi/\mu}, \tag{2}$$

in which Br is the Bradley number defined as a product of a ratio of the vent area, F, to the enclosure surface area, $V^{2/3}$, and a ratio of the speed of sound, c_{ui}, to flow velocity in front of the flame, $S_{ui}(E_i\text{-}1)$,

$$Br = \frac{F}{V^{2/3}} \cdot \frac{c_{ui}}{S_{ui}(E_i - 1)}, \tag{3}$$

where S_{ui} is the laminar burning velocity at initial conditions; E_i is the combustion products expansion coefficient at initial conditions; γ_u is the specific heat ratio for unburned mixture; π_0 is "pi" number; c_{ui} is the speed of sound at initial conditions of the deflagration; V is the enclosure volume; and χ/μ is the so-called deflagration-outflow interaction (DOI) number in which χ is the turbulence factor and μ is the generalised discharge coefficient that obey the Le Chatelier–Brown principle analogue for vented deflagrations [10, 11]. In 1999 correlation (1) the same empirical coefficients were applied to both hydrocarbon-air and hydrogen-air mixtures.

To meet requirements of standard development organisations the conservative form of the correlation was published in 2001 [6, 7] for hydrocarbon-air and hydrogen-air mixtures. This conservative correlation was updated in 2008 [9] for hydrogen-air mixtures only. For dimensionless reduced pressures below 1 the form of the conservative correlation 2008 is

$$\frac{\pi_{red}}{\pi_v^{2.5}} = 5.65 \cdot Br_t^{-2.5} \quad (\frac{\pi_{red}}{\pi_v^{2.5}} < 1), \tag{4}$$

where π_v is the dimensionless static activation pressure that is close to 1 for low-strength equipment and buildings and can be neglected. The conservative form of the correlation (4) between the dimensionless reduced pressure and turbulent Bradley number was validated against a wider range of vented deflagrations [7, 9] compared to the best fit correlation of 1999 [4]. The empirical coefficients for calculation of the DOI number were different for hydrocarbon-air and hydrogen-air mixtures in the 2001 correlation.

Referenced above vent sizing technique is proved to be a more accurate predictive tool with a wider range of applicability compared to current NFPA 68 [12] and CEN [13] standards based on the Bartknecht's equation and data [14]. This is achieved due to explicit introduction into the correlation of the effect of turbulence and combustion instabilities on the reduced deflagration pressure through the DOI number.

Vented deflagration is a complex combustion phenomenon that is characterised by a multiple pressure peak structure where each peak is governed by different combination of physical phenomena [15]. There are recent attempts [16] to calculate a magnitude of each peak of the multi-peak structure. This is a very important yet challenging task both scientifically and for engineering. Unfortunately, not all details of the study [16] are clear enough to be reproduced independently by safety engineers or researchers. The complexity of the problem can be demonstrated by the following experimental results. The experiments with lean hydrogen-air mixtures in vented enclosure of 120 m^3 volume by Kumar [17] demonstrated that though the maximum overpressure for central and near-vent ignition exhibits monotonic growth with hydrogen concentration in air, the maximum overpressure for the far-vent ignition first increases up to 9% hydrogen-air mixtures and then decreases significantly with a minimum at 10.3% and only then monotonically increases again with the concentration increase. It is expected that models like [16] have to explain and reproduce such experimental observations, including fourfold difference in overpressure for near- and far from the vent ignition of 9% hydrogen-air mixture, etc.

In this study the correlation is built using the maximum overpressure reported by experimentalists independent of which peak was prevailing and without distinction of the ignition source location. This obviously implies a larger scatter of experimental yet allows preserving the transparency of the correlation for engineers. Recent progress in understanding of large-scale premixed combustion and development of LES deflagration model [11] and the availability of the validation database formed of large-scale vented hydrogen-air deflagration experiments have paved a foundation for an essential upgrading of the correlation that is reported in this paper.

2. Experimental database for validation of the correlation

The widest range of experimental conditions for vented hydrogen-air deflagrations is applied in this study for the correlation validation. Validation experiments were carried out in enclosures of different shape with volume from 1 m^3 up to 120 m^3. Hydrogen concentration in air was in a range from very lean slow-burning mixtures with 6% by volume to near-stoichiometric fast-burning mixtures with hydrogen concentration up to 30% by volume. Ignition source location changed from the centre of enclosure to near and far from the vent. For the first time the correlation includes experimental data for both quiescent and iniatially turbulent mixtures. FM Global experiments with obstacles and ignition in the centre and far from the vent were processed as well.

Large-scale vented hydrogen-air deflagration experiments are used to validate the correlation. These validation experiments include: tests by Kumar in 120 m^3 volume enclosure both with quiescent and initially turbulent mixtures [17, 18]; tests performed by FM Global in 64 m^3 enclosure without and with obstacles [16, 19]; vented deflagration experiments carried out at INERIS in vented enclosures of 1 m^3 and 10 m^3 [20], early experiments by Pasman and colleagues in enclosure of 1 m^3 [21]. Data of 76 experiments are used to build the novel correlation and parameters of the experiments are given in Table 1 (see Appendix).

Experimental data in Table 1 include concentration of hydrogen in air, volume of enclosure, *V*, vent

area, F, ignition location, initial mixture temperature, T, initial burning velocity (corrected by the initial temperature), S_{ui}, dimensionless reduced pressure, π_{ed}, expansion coefficient of combustion products, E_i, speed of sound in the mixture at initial conditions, c_{ui}, critical radius for transition from laminar to fully turbulent self-similar flame propagation, R_0, maximum flame radius that is equal to a radius of spherical enclosure of equivalent volume, R, fluctuation or root mean square velocity, u'. Table 1 includes as well calculated by the technique described below the flame wrinkling factors for turbulence generated by flame front itself, Ξ_K, leading point mechanism, Ξ_{LP}, fractal increase of flame surface area, Ξ_{FR}, initial turbulence in the mixture, $\Xi_{u'}$, increase of flame surface area in elongated enclosure due to aspect ratio of the enclosure, Ξ_{AR}, accounting the presence of obstacles in enclosure, Ξ_O. Other parameters for each experiments in Table 1 are: empirical coefficient, ψ, that is described below, the DOI number, χ/μ, Bradley number, Br, and turbulent Bradley number, Br_t.

3. Previous studies of turbulent combustion generated during vented deflagrations

About forty years ago in 1975 Butlin concluded that turbulence should be studied in future works on vented deflagrations [22]. In 1978 Anthony underlined again that the production of an adequate mathematical model for vented deflagration would depend on resolving the problem of turbulence that in turn would allow the derivation of scaling laws for vented deflagrations [23].

It is well known that the venting of gases during deflagration facilitates the distortion of flame front due to different mechanisms. Various types of flame front instabilities such as hydrodynamic Darrieus-Landau instability and preferential diffusion instability, Rayleigh-Taylor and Kelvin-Helmholtz instabilities, flame cellular structure and fractal structure of turbulent flame surface, turbulence generated by flame front itself and by obstacles, initial flow turbulence before ignition, "external explosions" and large-scale flame front–flow interactions are some of these reasons. As a result, the burning rate, which is the product of the burning velocity by the flame surface area, in a vented vessel can exceed burning rate of laminar spherical flame up to 100 times, depending on conditions [7]. The *turbulence factor*, χ, is a widely accepted concept to characterise the augmentation of burning rate compared to the ideal case of laminar spherical flame propagation.

It is obvious that the turbulence factor, χ, is not a constant and changes in the course of vented deflagration. It can grow due to reasons mentioned in previous paragraph yet the turbulence factor can also decrease, e.g. due to flame laminarisation close to walls, flame extinction, etc. Nevertheless, usually a constant (averaged) turbulence factor is applied. This is a simplification stemming from the conclusion by Epstein et al. [24], who attempted to employ a variable turbulence factor in their analysis: "it seems best to employ a constant turbulence correction factor and gain the corresponding simplicity, rather than to carry more elaborate equations through a train of numerical computations whose accuracy is also limited to only a narrow range of experimental conditions".

The generalised discharge coefficient, μ, is dependent on vented deflagration conditions too. This fact was recognised about 30 years ago by different researchers. It has been demonstrated in a series of studies that reduced deflagration pressure correlates with the *deflagration-outflow interaction (DOI) number*, that is the ratio of the turbulence factor, χ, to the discharge coefficient, μ, rather than with the turbulence factor only. Tufano et al. [25] recommended the following correlation for the DOI number (*effective turbulence factor* in their terminology)

$$\chi / \mu = 0.51 \cdot \left[\frac{\mu FR}{V} \frac{c_{ui}}{S_{ui}} \sqrt{\frac{2}{\gamma - 1}} \right]^{0.6} \cdot \exp\left(- \frac{0.27}{\pi_v^3} \right), \tag{5}$$

where the dimensionless parameter in square brackets is quite close to the Bradley number in our studies determined by equation (3).

The inverse problem method for vented gaseous deflagrations was developed to find out the turbulence factor, χ, and the generalised discharge based, μ, for a particular experimental pressure dynamics [10]. The method was used over years allowing to gather data on venting generated turbulence. In particular, the analogue of the Le Chatelier-Brown principle for vented gaseous deflagrations was revealed through the application of this method to a wide range of experiments[10].

For the first time the correlation for turbulence generated by venting as a function of enclosure volume and Bradley number was presented in 1997 [26]. The DOI number correlation published in 1999 [4]

$$\chi / \mu = \alpha \cdot \left[\frac{(1 + e \cdot V_{\#}^{g}) \cdot (1 + 0.5 \cdot Br^{\beta})}{1 + \pi_v} \right]^{\delta} \cdot \pi_{i\#}^{\omega}, \quad (6)$$

where the empirical coefficients were α=0.9, β=1, δ=0.37, e=10, g=0.33, ω=0 for the best fit correlation of 1999 [4]; and α=1.00, β=0.8, δ=0.4, e=10, g=0.33, ω=0.6 for the conservative form of conservation of 2001 [6,7]. In 2008 the empirical coefficients in the correlation for DOI number were updated to α=1.00, β=0.8, δ=0.4, e=2, g=0.94, ω=0 [9].

The correlations for DOI number (5) and (6) are different in how they represent dependence on an enclosure size. The DOI number does not depend on the enclosure size following former correlation (5) by Tufano et al. [25] and increases with enclosure scale following our correlation (6) if the Bradley number or its analogy in correlation (5) are constant. It has been shown previously [5] that correlation (6) complies with the conclusion of Gouldin [27], who applied the fractal theory for turbulent flame modelling, that the flame surface of a turbulent outward propagating flame grows not as square of the flame radius, R^2, but faster as $R^2 R^{D-2}$. Here D is the fractal dimension which has theoretical value equal to 7/3 and measured value in the range 2.11-2.37 [11]. Indeed, both the correlation (6) derived as a result of processing of large amount of experimental pressure transients and the fractal-based approach with "additional growth" of flame surface area of R^{D-2} yield close to each other power dependences. The exponents in the DOI number dependence on the enclosure scale are 0.33 and 0.4 respectively. In contrast to the earlier correlation (5), the DOI number depends not only on the Bradley number (*venting parameter* in terminology of [25]) but also on the enclosure scale, $V^{1/3}$, as revealed in our previous studies. However, above mentioned correlations are of lumped parameter type and do not distinguish between different combustion instabilities and mechanisms in order to be more accurate in prediction of reduced pressure or vent sizing.

4. The correlation development using the multi-phenomena turbulent burning velocity model

Different in principle methodology to predict value of the DOI number is applied in this study The novel correlation is underpinned by the multi-phenomena turbulent burning velocity model which is used for Large Eddy Simulation (LES) of large-scale deflagration [11]. The model is under development during last decade. The following premixed combustion mechanisms and factors affecting the turbulent burning velocity are represented in the correlation on its own: turbulence generated by flame front itself, leading point mechanism stemming from the preferential diffusion in stretched flames, fractal increase of the flame surface area with flame size, initial turbulence in flammable mixture, enclosure aspect ratio, and presence of obstacles. Detailed description of the phenomena can be found elsewhere [11]. The ultimate equation for the DOI number accounting for these mechanisms and effects is drastically different from its previous form (6) and casts as

$$\chi / \mu = \Xi_K \cdot \Xi_{LP} \cdot \Xi_{FR} \cdot \Xi_{u'} \cdot \Xi_{AR} \cdot \Xi_O, \quad (7)$$

where the flame wrinkling factors due to various mechanisms affecting turbulent burning velocity are [11]: turbulence generated by flame front itself, Ξ_K; leading point factor, Ξ_{LP}; fractal increase of flame surface area, Ξ_{FR}; factor to account for initial turbulence, $\Xi_{u'}$; factor to account for increase of flame surface area due to enclosure elongation with growth of aspect ratio, Ξ_{AR}; and factor to account for increase of flame surface and turbulence in presence of obstacles in the enclosure Ξ_O. All wrinkling factors are equal to 1 for laminar flames and can grow above 1 for transitional and fully developed turbulent flames.

The factor Ξ_K accounts for the frame wrinkling due to so-called Karlovitz turbulence, i.e. turbulence generated by the flame front itself [28]. This type of tubulent combustion is different from the turbulent combustion when there is an initial turbulence in the flammable mixture approaching the flame front. It can be outlines as follows. Initially laminar flame first becomes cellular and wrinkles start to develop and split on an outward propagating flame. It is known that velocity of combustion products "leaving the flame front" is by an order of magnitude higher than velocity of flammable mixture entering the flame flame. These high speed jets of combustion products turbulise the wrinkled flame front as each jet hits oposite side of a flame wrinkle. The process developes until the flame becomes fully turbulent. It was shown that in an approximation that the turbulent burning velocity is equal to the fluctuating or root-mean squared (r.m.s.) velocity, the maximum theoretical value of flame wrinkling factor Ξ_K is equal to [11]

$$\Xi_K^{\max} = (E_i - 1) / \sqrt{3}, \quad (8)$$

where E_i is the combustion products expansion coefficient.

Gostintsev et al [29] reported that for stoichiometric hydrogen-air mixtures the transition from laminar to self-similar (fractal) fully turbulent flame propagation regime takes place in quescent mixture at a characteristic distance from an ignition source of about R_0 =1.0-1.2 m. Unfortunately, there is no data that authors are familiar with on a characteristic flame radius for lean hydrogen-air mixtures.

Thus, based on the theory by Karlovitz et al. [28] and observations by Gostintsev et al. [29] the following equation for turbulence generated by flame front itself was suggested [11]

$$\Xi_K = 1 + \left(\psi \cdot \Xi_K^{\max} - 1\right) \cdot \left[1 - \exp\left(-R/R_0\right)\right], \tag{9}$$

where R is the flame radius; R_0 is the characteristic flame radius for transition from laminar to fully turbulent flame; Ξ_K^{max} is the theoretical maximum of the Karlovitz wrinkling factor, Ξ_K; ψ is the empirical coefficient indicating how closely the maximum value of this wrinkling factor Ξ_K^{max} can be reached depending on hydrogen concentration in the mixture. For the purpose of this paper the maximum flame radius R is restricted by the enclosure scale, independenly of its shape, and is calculated from the enclosure volume, V, as

$$R = \sqrt[3]{3V/4\pi}\,. \tag{10}$$

The characteristic radius R_0 as a function of hydrogen mole fraction in hydrogen-air mixture was assumed in this study, based on the understanding of underlying physical phenomena and CFD simulation of lean hydrogen-air deflagrations, as shown in Fig. 1 (left). For near stoichiometric and rich hydrogen-air mixtures with hydrogen concentration more than 20% by volume and up to the upper flammability limit of 75% by volume the transition to fully developed turbulent flame takes place at R_0=1.2 m. It is assumed in this study that for lean hydrogen-air mixtures prone to thermo-diffusive instability the characteristic radius decreases with concentration. For mixtures with hydrogen concentration below 20% by volume down to the lower flammability limit for upward flame propagation of 4% by volume this dependence is assumed in this study as $R_0 = -0.12 + 6.7X$.

Previous studies demonstrated that the empirical coefficient ψ depends on the hydrogen mole fraction in air. The coefficient approaches its limit ψ=1 for very lean mixtures and is about ψ=0.5 for stoichiometric and rich mixtures [11]. Indeed, lean mixtures are subject to thermo-diffusive instability and burn slower. This increases chances to achieve isotropic turbulent combustion and thus for Karlovitz turbulence to reach its theoretical maximum. The functional dependence of ψ is generalised in Fig. 1 (right). The coefficient ψ=1 for hydrogen mole fraction X=0.04-0.20, and ψ=0.5 for hydrogen mole fraction X=0.30-0.75. It changes linearly between this two limits in the range of mole fractions X=0.20-0.30.

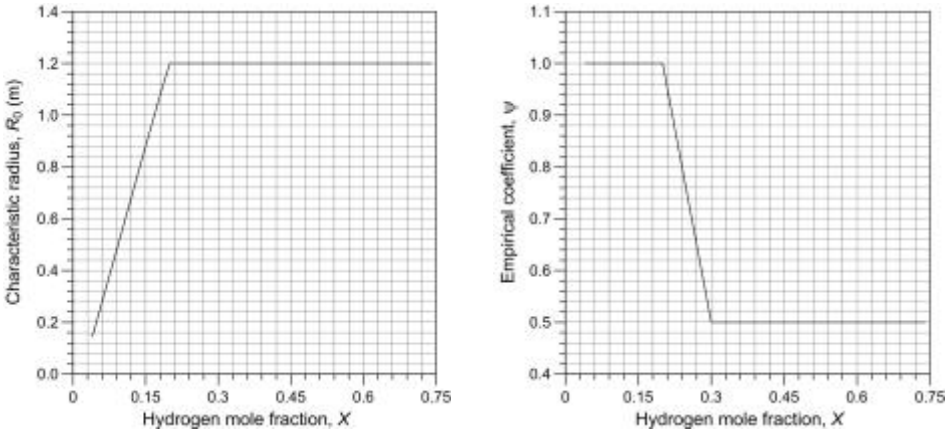

Figure 1. The characteristic flame radius R_0 as a function of hydrogen mole fraction (left). The empirical coefficient ψ as a function of hydrogen mole fraction (right).

Wrinkling factor Ξ_{LP} accounts for the effect of preferential diffusion of hydrogen compared to air in stretched (curved and strained) flames, which is important for lean hydrogen-air premixed combustion and can be neglected for rich mixtures. The concept of leading point can be oulined as follows. Turbulent flame has instabilities of different curvature. There is only one flame curvature for which, in presence of the preferencial diffusion, a mass burning rate reaches its maximum compared to flamelets

of smaller or larger curvature. The flamelets with such cirvature will propagate faster and lead the turbulent flame propagation. They are called leading points. It was observed in HySAFER CFD studies and suggested that the leading point flame wrinkling factor Ξ_{LP} develops linearly with radius and reaches its maximum at half of the characteristic radius R_0 for Karlovitz turbulence and remains constant after this [11]. The leading point wrinkling factor chages lenearly with radius from 1 to its maximum at $R_0/2$ as

$$\Xi_{LP} = 1 + \frac{\left(\Xi_{LP}^{\max} - 1\right) \cdot 2R}{R_0}, \tag{11}$$

where Ξ_{LP}^{max} is the maximum leading point wrinkling factor that is a function of hydrogen mole fraction. This functional dependence is shown in Fig. 2 (left) [30].

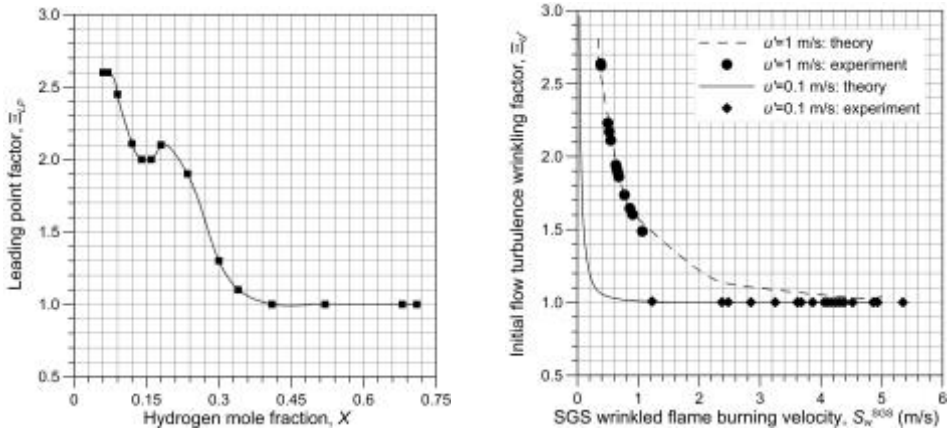

Figure 2. Left: the maximum leading point wrinkling factor Ξ_{LP}^{max} as a function of hydrogen mole fraction [30]. Right: The initial flow turbulence wrinkling factor $\Xi_{u'}$ as a function of the SGS wrinkled flame burning velocity S_w^{SGS} for experiments with initial turbulence u'=0.1 m/s (Bauwens et al., [16, 19]) and u'=1 m/s (Kumar, [18]).

It is known from experimental observations and CFD simulations that premixed flame propagating within an enclosure tends to get a shape of the enclosure. The factor Ξ_{AR} accounts for the increase of flame front surface area due to the enclosure elongation (aspect ratio more than 1) and is defined in this study as

$$\Xi_{AR} = A_{EW} / A_S, \tag{12}$$

where A_{EW} is the internal surface area of an enclosure, and A_S is the area of the sphere of the same volume with radius R calculated using Eq. 10.

Turbulent flame surface area is corrugated and for outward propagating flame its radius (outter cut-off) is growing in time. Wrinkling factor Ξ_{FR} accounts for the fractal increase of the flame front area with increase of flame radius (outer cut-off). In particular, it was demonstrated that this mechanism is responsible for flame acceleration during large-scale deflagrations in the open atmosphere [31]. This mechanism of burning rate augmentation is definitely applied when flame is already turbulent, i.e. when the flame radius greater than R_0 according to conclusions by Gostintsev et al [29]. The wrinkling factor Ξ_{FR} is applied in this study only when an enclosure size is more than characteristic radius, $R > R_0$, and is calculated as [31]

$$\Xi_{FR} = \left(R / R_0\right)^{D-2}, \tag{13}$$

where D is the fractal dimension taken here as equal to its theoretical value of D=2.33.

While basic research is focused on deflagrations in initially quescent mixtures to understand the fundamentals of involved phenomena, in many practical situations the flammable mixture could be agitated before ignition, e.g. by a jet of leaking hydrogen. Wrinkling factor $\Xi_{u'}$ accounts for initial turbulence in the flammable mixture. This is done through the modified Yakhot's transcendental equation for turbulent burning velocity, S_t, [11, 32]

$$S_t = S_w^{SGS} \cdot \exp\left(u' / S_t\right)^2, \tag{14}$$

where S_w^{SGS} is the sub-grid scale (SGS) wrinkled flame burning velocity; and u' is the r.m.s. velocity.

The principal modification of the Yakhot's original equation is substitution of laminar burning velocity, S_u, by the unresolved SGS wrinkled flame velocity that is affected by all other combustion mechanisms except the effect of initial turbulence [11]. The maximum overpressure in the vented enclosure during deflagration is defined by the largest burning rate that is achieved by the end of combustion when the flame approaches the enclosure walls and reaches its maximum. At this moment the burning rate is affected by different mechanisms discussed above, including the aspect ratio. Thus, in the Yakhot's original equation the value of laminar burning velocity S_u has to be substituted by the SGS wrinkled flame velocity

$$S_w^{SGS} = S_u \cdot \Xi_K \cdot \Xi_{LP} \cdot \Xi_{FR} \cdot \Xi_{AR} \cdot \Xi_O, \qquad (15)$$

The available data on initially turbulent hydrogen-air deflagrations is limited, so the approach is applied for two levels of initial turbulence available: u'=0.1 m/s (FM Global experiments [16, 19]) and u'=1 m/s (Kumar tests [18]). The characteristic values of the turbulence factor $\Xi_{u'}$ are shown in Fig. 2 (right) for experiments by Bauwens et al [16, 19] and Kumar [18]. The values of the SGS wrinkled flame burning velocity S_w^{SGS} are plotted on the abscissa in Fig. 2 (right). Lines represent theoretical curves given by the modified Yakhot equation for turbulent burning velocity (14) and symbols represent values calculated for experiments by Bauwens et al [16, 19] for u'=0.1 m/s and Kumar [18] for u'=1 m/s. Values of $\Xi_{u'}$ were calculated as ratio of S_t to S_w^{SGS}, where S_t was calculated from Eq. (14) with S_w^{SGS} calculated from Eq. (15) with all wrinkling factors calculated at the end of deflagration when flame radius is equal to the enclosure equivalent radius.

Figure 2 (right) demonstrates that for S_w^{SGS} of 0.35 m/s and initial turbulence 1 m/s the wrinkling factor is $\Xi_{u'}$=2.8, and for initial turbulence 0.1 m/s it is only $\Xi_{u'}$=1.007. The lower burning velocity the higher the turbulence factor. For example, for the lowest burning rate at the lower flammability limit of S_u=0.032 m/s the theoretical wrinkling factor due to initial turbulence is $\Xi_{u'}$=18 and $\Xi_{u'}$=3 for u'=1 m/s and u'=0.1 m/s respectively.

Experiments studying effect of obstacles on hydrogen-air deflagration dynamics are very limited. There is data on four experiments with obstacles taken from FM Global paper [16], three of which are for central ignition and one for ignition at rear wall. For central ignition and obstacles present in FM Global experiments there is practically no effect of obstacles on vented deflagration overpressure compared to experiments without obstacles. Thus, for this configuration Ξ_O = 1 was taken. The wrinkling factor for the fourth experiment with rear ignition, when obstacles are between the ignition source and the vent, it is found that Ξ_O = 3.5 to match the correlation without obstacles. More experimental data and analysis is needed to derive a functional dependence of vented deflagration overpressure on parameters, number and respective location of ignition source, obstacles, and a vent.

All 76 processed experimental data on vented hydrogen-air deflagrations (see Table 1 in Appendix) are presented in Fig. 3 (left) in coordinates "dimensionless reduced pressure – turbulent Bradley number". Data are characteristic for low-strength equipment and buildings, i.e. applied for $\pi_{red} < 1$. The best fit and conservative equations (conservative across the complete range of experiments) are respectively

$$\pi_{red} = 0.33 \cdot Br_t^{-1.3} \text{ (best fit)}, \qquad \pi_{red} = 0.86 \cdot Br_t^{-1.3} \text{ (conservative)}. \qquad (16)$$

The conservative estimate of reduced pressure is 2.6 times higher compared to the best fit estimate.

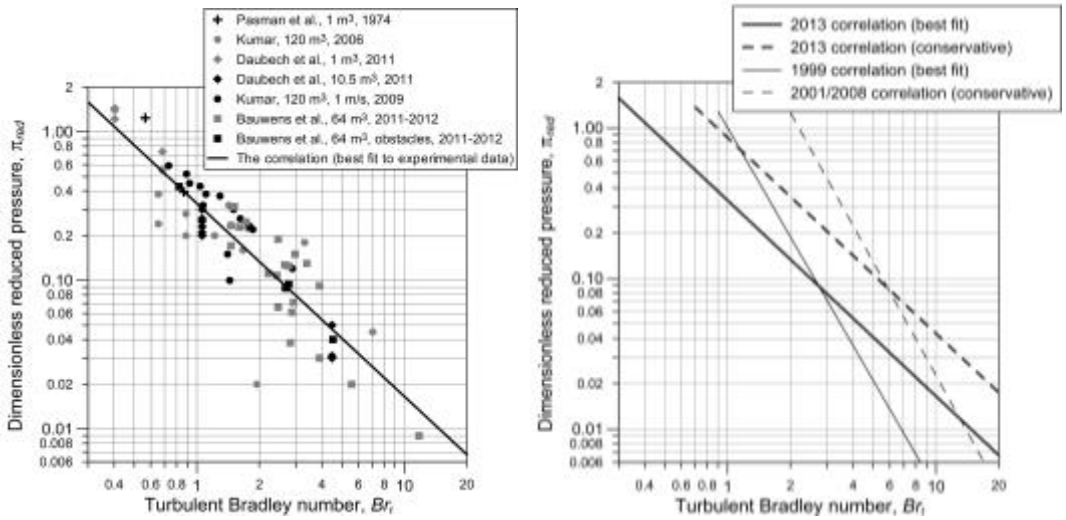

Figure 3. Left: novel correlation (best fit line) against experimental data (76 points). Right: novel correlation (best fit and conservative) against 1999 correlation (best fit) [4] and 2001/2008 correlation (conservative) [6, 7, 9].

5. Predictive capability compared to former correlations

Figure 4 (right) shows comparison between the novel correlation, both best fit and conservative lines are shown, and previous best fit correlation of 1999 [4] and conservative correlation of 2001/2008 [6, 7, 9]. The slope of new correlation is not so steep relative to former correlations. Former correlations overpredict reduced pressure above 9 kPa, and underpredict below 9 kPa. Both cases imply additional safety costs. The reduced pressure "sensitivity" to value of turbulent Bradley number is improved due to the integration of recent knowledge on premixed combustion during vented deflagrations [11] and wider range of experimental data applied in this study. The predictive accuracy of the correlation is enhanced and difference between the best fit and the conservative curves reduced from former 5.3 times to 2.6 in this study. This is an essential improvement in the correlation predictive capability.

6. Vent sizing technique

The correlation can be used both ways, i.e. to calculate the vent area required to reduce deflagration pressure to a given level, or to estimate an overpressure for a vent of known size. The procedure for calculating the vent area of an enclosure fully filled by a hydrogen-air mixture of known concentration is as follows:

- Calculate the value of dimensionless reduced deflagration pressure $\pi_{red} = (P_{max} - P_i) / P_i$, where P_{max} is the maximum absolute pressure that the enclosure can withstand, and P_i is the initial absolute pressure (P_{max} and P_i should have the same units);
- Based on the value of π_{red}, calculate the value of Br_t by using the relevant Eq. (16), i.e. the best fit or the conservative, or calculate graphically using the correlation in Fig. 3 (left);
- Determine graphically values of initial laminar burning velocity, S_{ui}, and combustion products expansion coefficient, E_i, for a given hydrogen mole fraction in air (see Fig. 4, left and right);
- Compute all flame wrinkling factors as described above and multiply them to get the DOI number, χ/μ, from Eq. (7) $\chi/\mu = \Xi_K \cdot \Xi_{LP} \cdot \Xi_{FR} \cdot \Xi_{u'} \cdot \Xi_{AR} \cdot \Xi_O$;
- Finally, determine the vent area by the following equation

$$F = Br_t \cdot \frac{\chi}{\mu} \cdot \sqrt[3]{36\pi_0} \cdot V^{2/3} \cdot \frac{S_{ui} \cdot (E_i - 1)}{c_{ui} \cdot \sqrt{E_i / \gamma_u}}. \quad (17)$$

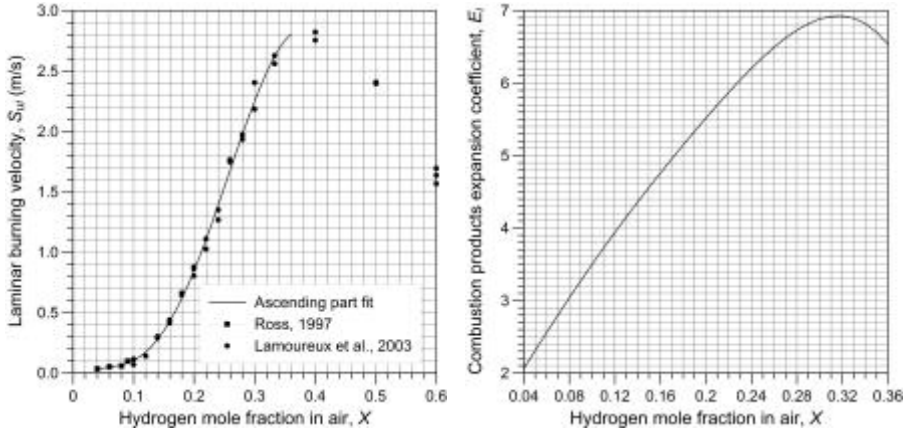

Figure 4. Laminar burning velocity S_{ui} (left) and expansion coefficient of combustion products E_i (right) as functions of hydrogen mole fraction in air, X.

The correlation was calibrated against experimental data using the dependence of burning velocity on hydrogen concentrations in air by combining data from Ross [33] for lean mixtures with concentration less than 10% by volume of hydrogen, and Lamoureux [34] for mixtures with concentration above 10% by volume (unstretched data are taken from [34]).

7. Future research

The effect of "external explosion" on reduced pressure has to be accounted for explicitly by an appropriate model when a better understanding of the phenomenon is gained. The model has to reproduce the experimentally observed strong effect of ignition source location on reduced pressure for different lean hydrogen-air mixtures as shown in Fig. 5 (left) [17]. One possible reason of this "effect" could be the experimental scatter of laminar burning velocity for ultra-lean mixtures (Fig. 5, right).

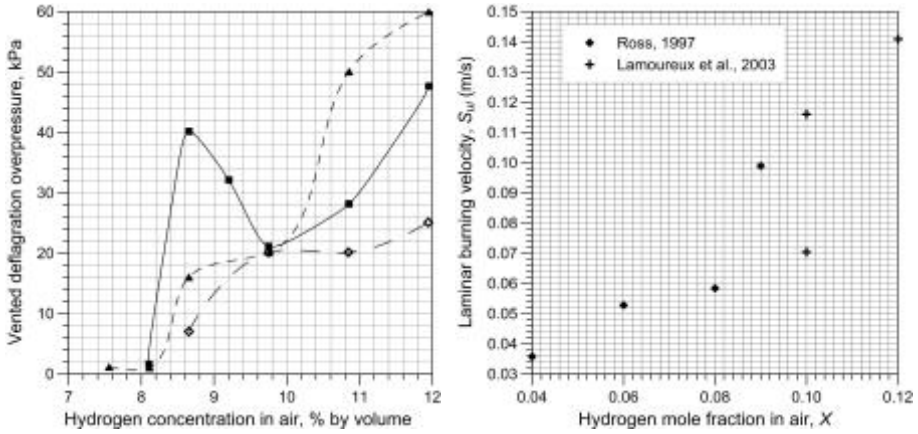

Figure 5. The effect of ignition source location on reduced pressure for different lean hydrogen-air mixtures (left) [17]. The scattering of laminar burning velocity for ultra-lean hydrogen-air mixtures (right).

It should be noted that none of the experiments collated in the Table 1 had a deflagration-to-detonation transition during venting, for which higher levels of overpressure could be reached. This phenomenon is not considered in this paper and available correlations for deflagration venting do not take it into account.

8. Conclusions

The novel correlation for vented hydrogen-air deflagrations is presented that incorporates the explicit introduction into the deflagration-outflow interaction (DOI) a number of phenomena affecting turbulent burning velocity. The equations are simple algebraic formulae that can be easily used by safety engineers to program a simple tool for vent sizing. The correlation is applicable to low-strength equipment and buildings with overpressure below 0.1 MPa, and validated against the widest range of large-scale hydrogen-air vented deflagrations data available up to date.

Acknowledgements

*

Authors are grateful to the Fuel Cells and Hydrogen Joint Undertaking for funding the research leading to this publication through the HyIndoor project (grant agreement No. 278534).

References

1. Sustek J, Janovsky B. Comparison of empirical and semi empirical equations for vented gas explosions with experimental data. In: Proceedings of the 9th International Symposium of Hazards, Prevention and Mitigation of Industrial Explosions, 22-27 July 2012, Cracow, Poland.
2. Molkov VV. Theoretical generalization of international experimental data on vented explosion dynamics. In: Proceedings of the First International Seminar on Fire and Explosion Hazard of Substances and Venting of Deflagrations, 17-21 July 1995, Moscow, pp.166-181.
3. Molkov VV, Korolchenko AYa, Alexandrov SV. Venting of deflagrations in buildings and equipment: universal correlation. In: Proceedings of the Fifth International Symposium on Fire Safety Science, 3-7 March 1997, Melbourne, 1997, pp.1249-1260.
4. Molkov VV, Dobashi R, Suzuki M, Hirano T. Modelling of Vented hydrogen-air deflagrations and correlations for vent sizing. Journal of Loss Prevention in the Process Industries 1999;12:147-156.
5. Molkov VV, Dobashi R, Suzuki M, Hirano T. Venting of deflagrations: hydrocarbon-air and hydrogen-air systems. Journal of Loss Prevention in the Process Industries 2000;13(3-5):397-409.
6. Molkov VV. Unified correlations for vent sizing of enclosures at atmospheric and elevated pressures. Journal of Loss Prevention in the Process Industries 2001;14:567-574.
7. Molkov VV. Turbulence generated during vented gaseous deflagrations and scaling issue in explosion protection, In: IChemE Symposium Series, 2001;148:279-292.
8. Molkov VV. Accidental gaseous deflagrations: modelling, scaling and mitigation, Journal de Physique IV 2002;12:7-19 – 7-30.
9. Molkov V, Verbecke F, Saffers J-B. Uniform hydrogen-air deflagrations in vented enclosures and tunnels: predictive capabilities of engineering correlations and LES. In: Proceedings of the 7th International Symposium on Hazards, Prevention and Mitigation of Industrial Explosions, 6-12 July 2008, St-Petersburg, 2:158-167.
10. Molkov VV, Baratov AN, Korolchenko AYa. Dynamics of gas explosions in vented vessels: A critical review and progress. Progress in Astronautics and Aeronautics, Vol. 154 "Dynamics aspects of Explosion Phenomena", Proceedings of the 13th International Colloquium on Dynamics of Explosions and Reactive Systems, 1991, Nagoya - Japan, 1993, pp.117-131.
11. Molkov V. Fundamentals of Hydrogen Safety Engineering (Part 1 and 2). www.bookboon.com. http://bookboon.com/en/textbooks/mechanics/fundamentals-of-hydrogen-safety-engineering-i and http://bookboon.com/en/textbooks/mechanics/fundamentals-of-hydrogen-safety-engineering-ii.
12. NFPA 68, 2007. Standard on Explosion Protection by Deflagration Venting, *National Fire Protection Association*, NFPA, 1 Batterymarch Park, Quincy, Massachusetts, USA 02169-7471.
13. EN 14994: 2007. Gas Explosion Venting Protective Systems.
14. Bartknecht W. Explosions-Schutz: Grundlagen und Anwendung, Springer-Verlag, 1993.
15. Cooper MG, Fairweather M, Tite JP. On the mechanism of pressure generation in vented explosions. Combustion and Flame 1986;65:1-14.
16. Bauwens CR, Chao J, Dorofeev SB. Effect of hydrogen concentration on vented explosion overpressures from lean hydrogen-air deflagrations. International Journal of Hydrogen Energy 2012;37:17599-17605.
17. Kumar RK. Vented combustion of hydrogen-air mixtures in a large rectangular volume. In: 44th AIAA Aerospace Sciences Meeting and Exhibit, 9-12 January 2006, Reno, USA, Paper AIAA 2006-375.
18. Kumar RK. Vented turbulent combustion of hydrogen-air mixtures in a large rectangular volume. In: 47th AIAA Aerospace Sciences Meeting Including The New Horizons Forum and Aerospace Exposition, 5-8 January 2009, Orlando, USA, Paper AIAA 2009-1380.
19. Bauwens CR, Chaffee J, Dorofeev SB. Vented explosion overpressures from combustion of hydrogen and hydrocarbon mixtures. International Journal of Hydrogen Energy 2011;36:2329-2336.
20. Daubech J, Proust C, Jamois D, Leprette E. Dynamics of vented hydrogen-air deflagrations. In: Proceedings of the 4th International Conference on Hydrogen Safety, 12-14 September 2011, San Francisco, USA. Paper 236.

*

21. Pasman HJ, Groothuisen ThM, Gooijer PH. Design of Pressure Relief Vents. In: Loss Prevention and Safety Promotion in the Process Industries (Buschman CH, Ed.). In: Proceedings of the First International Loss Prevention Symposium, Delft, Netherlands. 1974.
22. Butlin RN. A review of information on experiments concerning the venting of gas explosions in buildings. Fire Research Note 1975; No.1026, 19 p.
23. Anthony EJ. The use of venting formulae in the design and protection of building and industrial plant from damage by gas or vapour explosions. Journal of Hazardous Materials 1977/78; 2:23-49.
24. Epstein M, Swift I, Fauske HK. Estimation of peak pressure for sonic-vented hydrocarbon explosions in spherical vessels. Combustion and Flame 1986; 66:1-8.
25. Tufano V, Crescitelli S, Russo G. On the design of venting systems against gaseous explosions. Journal of Occupational Accidents 1981; 3:143-152.
26. Molkov VV. Scaling of turbulent vented deflagrations. In: Proceedings of the Second International Seminar on Fire and Explosion Hazards, 10-15 August 1997, Moscow, Russia, pp.445-456.
27. Gouldin FC. An application of fractals to modeling premixed turbulent flames. Combustion and Flame 1987; 68:249-266.
28. Karlovitz B, Denniston DWJr, Wells FE. Investigation of turbulent flames. The Journal of Chemical Physics 1951;19(5):541-547.
29. Gostintsev YuA, Istratov AG, Shulenin YuV. Self-similar propagation of a free turbulent flame in mixed gas mixtures. Combustion, Explosion and Shock Waves 1988;24(5):63-70.
30. Verbecke F. Formation and combustion of non-uniform hydrogen-air mixtures. PhD Thesis, University of Ulster, Belfast, UK, 2009.
31. Molkov VV, Makarov DV, Schneider H. LES modelling of an unconfined large-scale hydrogen-air deflagration. Journal of Physics D: Applied Physics 2006;39:4366-4376.
32. Yakhot V. Propagation velocity of premixed turbulent flames. Combustion Science and Technology 1988;60: 191-214.
33. Ross MC. Lean combustion characteristics of hydrogen-nitrous oxide-ammonia mixtures in air. MEng Thesis. California Institute of Technology, Pasadena, California, USA, 1997.
34. Lamoureux N, Djebaili-Chaumeix N, Paillard C-E. Flame velocity determination for H_2-air-He-CO_2 mixtures using the spherical bomb. Experimental Thermal and Fluid Science 2003;27:385-393.

*

Appendix.

Table 1. Experimental data, calculated wrinkling factors and other parameters for 76 experiments used to build the novel correlation.

Test	H_2, % vol.	V, m^3	F, m^2	Ign[a]	T, K	S_{ui} [b], m/s	π_{red} [c]	E_i	c_{ui}	R_0	R	Ξ_K^{max}	ψ	Ξ_K	Ξ_{AR}	Ξ_{LP} [e]	Ξ_{FR}	u', m/s	$\Xi_{u'}$	Ξ_O	χ/μ	Br	Br_t
K-8.5-C [17]	8.5	120	0.55	C	301	0.08	0.02	3.16	363	0.45	3.06	1.25	1.00	1.24	1.39	2.41	1.88	0.00	1.00	1.00	7.85	49.21	1.95
K-9-N [17]	9	120	0.55	N	301	0.09	0.07	3.27	364	0.49	3.06	1.31	1.00	1.31	1.39	2.38	1.84	0.00	1.00	1.00	7.97	42.08	1.67
K-9-C [17]	9	120	0.55	C	301	0.09	0.16	3.27	364	0.49	3.06	1.31	1.00	1.31	1.39	2.38	1.84	0.00	1.00	1.00	7.97	42.08	1.67
K-9-R-1 [17]	9	120	0.55	R	301	0.09	0.40	3.27	364	0.49	3.06	1.31	1.00	1.31	1.39	2.38	1.84	0.00	1.00	1.00	7.97	42.08	1.67
K-9-R-2 [17]	9	120	1.09	R	301	0.09	0.18	3.27	364	0.49	3.06	1.31	1.00	1.31	1.39	2.38	1.84	0.00	1.00	1.00	7.97	83.39	3.31
K-9-R-3 [17]	9	120	2.19	R	301	0.09	0.03	3.27	364	0.49	3.06	1.31	1.00	1.31	1.39	2.38	1.84	0.00	1.00	1.00	7.97	167.54	6.64
K-9.5-R [17]	9.5	120	0.55	R	301	0.10	0.32	3.39	365	0.52	3.06	1.38	1.00	1.38	1.39	2.34	1.79	0.00	1.00	1.00	8.08	35.84	1.43
K-10-N [17]	10	120	0.55	N	301	0.11	0.20	3.50	366	0.55	3.06	1.44	1.00	1.44	1.39	2.31	1.76	0.00	1.00	1.00	8.17	30.45	1.22
K-10-C [17]	10	120	0.55	C	301	0.11	0.20	3.50	366	0.55	3.06	1.44	1.00	1.44	1.39	2.31	1.76	0.00	1.00	1.00	8.17	30.45	1.22
K-10-R [17]	10	120	0.55	R	301	0.11	0.21	3.50	366	0.55	3.06	1.44	1.00	1.44	1.39	2.31	1.76	0.00	1.00	1.00	8.17	30.45	1.22
K-11-N [17]	11	120	0.55	N	301	0.14	0.20	3.72	368	0.62	3.06	1.57	1.00	1.57	1.39	2.25	1.69	0.00	1.00	1.00	8.33	21.93	0.89
K-11-C [17]	11	120	0.55	C	301	0.14	0.50	3.72	368	0.62	3.06	1.57	1.00	1.57	1.39	2.25	1.69	0.00	1.00	1.00	8.33	21.93	0.89
K-11-C-Max [17]	11	120	0.55	C	301	0.14	0.28	3.72	368	0.62	3.06	1.57	1.00	1.57	1.39	2.25	1.69	0.00	1.00	1.00	8.33	21.93	0.89
K-11-R [17]	11	120	0.55	R	301	0.14	0.28	3.72	368	0.62	3.06	1.57	1.00	1.57	1.39	2.25	1.69	0.00	1.00	1.00	8.33	21.93	0.89
K-12-N [17]	12	120	0.55	N	301	0.18	0.24	3.94	370	0.69	3.06	1.70	1.00	1.69	1.39	2.19	1.64	0.00	1.00	1.00	8.44	15.89	0.65
K-12-C [17]	12	120	0.55	C	301	0.18	0.60	3.94	370	0.69	3.06	1.70	1.00	1.69	1.39	2.19	1.64	0.00	1.00	1.00	8.44	15.89	0.65
K-12-C-Max [17]	12	120	0.55	C	301	0.18	0.38	3.94	370	0.69	3.06	1.70	1.00	1.69	1.39	2.19	1.64	0.00	1.00	1.00	8.44	15.89	0.65
K-12-R [17]	12	120	0.55	R	301	0.18	0.48	3.94	370	0.69	3.06	1.70	1.00	1.69	1.39	2.19	1.64	0.00	1.00	1.00	8.44	15.89	0.65
INERIS-1.01-01 [20]	27	1	0.15	R	295	1.80	1.40	6.62	399	1.20	0.62	3.25	0.65	1.45	3.18	1.43	1.00	0.00	1.00	1.00	6.59	5.91	0.40
INERIS-1.01-02 [20]	27	1	0.15	R	295	1.80	1.22	6.62	399	1.20	0.62	3.25	0.65	1.45	3.18	1.43	1.00	0.00	1.00	1.00	6.59	5.91	0.40
INERIS-1.01-03 [20]	27	1	0.15	R	295	1.80	1.44	6.62	399	1.20	0.62	3.25	0.65	1.45	3.18	1.43	1.00	0.00	1.00	1.00	6.59	5.91	0.40
INERIS-1.01-04 [20]	20	1	0.15	R	295	0.83	0.73	5.52	382	1.20	0.62	2.61	1.00	1.65	3.18	1.75	1.00	0.00	1.00	1.00	9.17	15.27	0.68
INERIS-1.01-05 [20]	20	1	0.15	R	295	0.83	0.55	5.52	382	1.20	0.62	2.61	1.00	1.65	3.18	1.75	1.00	0.00	1.00	1.00	9.17	15.27	0.68
INERIS-1.01-06 [20]	15	1	0.15	R	295	0.34	0.23	4.56	372	0.89	0.62	2.06	1.00	1.53	3.18	2.02	1.00	0.00	1.00	1.00	9.79	45.93	1.75
INERIS-1.01-07 [20]	15	1	0.15	R	295	0.34	0.24	4.56	372	0.89	0.62	2.06	1.00	1.53	3.18	2.02	1.00	0.00	1.00	1.00	9.79	45.93	1.75
INERIS-1.01-08 [20]	10	1	0.15	R	295	0.10	0.04	3.50	362	0.55	0.62	1.44	1.00	1.30	3.18	2.31	1.04	0.00	1.00	1.00	9.91	212.89	7.03
INERIS-10.5-11 [20]	14	10.5	2.00	R	295	0.27	0.03	4.36	370	0.82	1.36	1.94	1.00	1.76	3.18	2.07	1.18	0.00	1.00	1.00	13.67	168.03	4.49
INERIS-10.5-12 [20]	14	10.5	2.00	R	295	0.27	0.05	4.36	370	0.82	1.36	1.94	1.00	1.76	3.18	2.07	1.18	0.00	1.00	1.00	13.67	168.03	4.49
INERIS-10.5-13 [20]	14	10.5	2.00	R	295	0.27	0.03	4.36	370	0.82	1.36	1.94	1.00	1.76	3.18	2.07	1.18	0.00	1.00	1.00	13.67	168.03	4.49
INERIS-10.5-16 [20]	23	10.5	2.00	R	295	1.23	0.23	6.04	389	1.20	1.36	2.91	0.85	2.00	3.18	1.61	1.04	0.00	1.00	1.00	10.64	26.28	1.06
INERIS-10.5-17 [20]	23	10.5	2.00	R	295	1.23	0.21	6.04	389	1.20	1.36	2.91	0.85	2.00	3.18	1.61	1.04	0.00	1.00	1.00	10.64	26.28	1.06
INERIS-10.5-19 [20]	23	10.5	2.00	R	295	1.23	0.20	6.04	389	1.20	1.36	2.91	0.85	2.00	3.18	1.61	1.04	0.00	1.00	1.00	10.64	26.28	1.06
INERIS-10.5-20 [20]	23	10.5	2.00	R	295	1.23	0.25	6.04	389	1.20	1.36	2.91	0.85	2.00	3.18	1.61	1.04	0.00	1.00	1.00	10.64	26.28	1.06
INERIS-10.5-21 [20]	23	10.5	2.00	R	295	1.23	0.20	6.04	389	1.20	1.36	2.91	0.85	2.00	3.18	1.61	1.04	0.00	1.00	1.00	10.64	26.28	1.06
INERIS-10.5-22 [20]	23	10.5	2.00	R	295	1.23	0.26	6.04	389	1.20	1.36	2.91	0.85	2.00	3.18	1.61	1.04	0.00	1.00	1.00	10.64	26.28	1.06
INERIS-10.5-23 [20]	23	10.5	2.00	R	295	1.23	0.30	6.04	389	1.20	1.36	2.91	0.85	2.00	3.18	1.61	1.04	0.00	1.00	1.00	10.64	26.28	1.06
K-5.9-C-T [18]	5.9	120	0.55	C	298	0.05	0.10	2.53	357	0.28	3.06	0.88	1.00	1.00	1.39	2.58	2.21	1.00	2.64	1.00	20.95	108.59	1.44
K-6.1-C-T [18]	6.1	120	0.55	C	298	0.05	0.15	2.58	357	0.29	3.06	0.91	1.00	1.00	1.39	2.57	2.18	1.00	2.62	1.00	20.40	102.28	1.41

*

K-7.8-C-T [18]	7.8	120	0.55	C	298	0.07	0.38	2.99	360	0.41	3.06	1.15	1.00	1.15	1.39	2.45	1.95	1.00	2.23	1.00	17.09	62.55	1.11
K-8-C-T [18]	8	120	0.55	C	298	0.07	0.32	3.04	360	0.42	3.06	1.18	1.00	1.18	1.39	2.44	1.93	1.00	2.17	1.00	16.75	58.93	1.07
K-8.2-C-T [18]	8.2	120	0.55	C	298	0.07	0.43	3.09	361	0.43	3.06	1.20	1.00	1.20	1.39	2.43	1.91	1.00	2.11	1.00	16.41	55.48	1.04
K-8.9-C-T [18]	8.9	120	0.55	C	298	0.08	0.45	3.25	362	0.48	3.06	1.30	1.00	1.30	1.39	2.38	1.84	1.00	1.91	1.00	15.22	44.63	0.92
K-9.1-C-T [18]	9.1	120	0.55	C	298	0.09	0.52	3.30	362	0.49	3.06	1.33	1.00	1.32	1.39	2.37	1.83	1.00	1.86	1.00	14.88	41.88	0.89
K-10.2-C-T [18]	10.2	120	0.55	C	298	0.11	0.59	3.55	365	0.57	3.06	1.47	1.00	1.47	1.39	2.30	1.74	1.00	1.60	1.00	13.16	29.26	0.73
K-8.8-C-T [18]	8.8	120	1.09	C	298	0.08	0.22	3.23	362	0.47	3.06	1.29	1.00	1.29	1.39	2.39	1.85	1.00	1.94	1.00	15.39	91.30	1.86
K-9-C-T [18]	9	120	1.09	C	298	0.08	0.23	3.27	362	0.49	3.06	1.31	1.00	1.31	1.39	2.38	1.84	1.00	1.89	1.00	15.05	85.69	1.80
K-9.6-C-T [18]	9.6	120	1.09	C	298	0.10	0.26	3.41	363	0.53	3.06	1.39	1.00	1.39	1.39	2.34	1.79	1.00	1.74	1.00	14.07	70.61	1.62
K-10-C-T [18]	10	120	1.09	C	298	0.11	0.30	3.50	364	0.55	3.06	1.44	1.00	1.44	1.39	2.31	1.76	1.00	1.65	1.00	13.45	61.93	1.51
K-10.8-C-T [18]	10.8	120	1.09	C	298	0.13	0.37	3.68	366	0.61	3.06	1.55	1.00	1.54	1.39	2.26	1.70	1.00	1.49	1.00	12.35	47.58	1.29
K-10-C-T-2 [18]	10	120	2.09	C	298	0.11	0.12	3.50	364	0.55	3.06	1.44	1.00	1.44	1.39	2.31	1.76	1.00	1.65	1.00	13.45	118.75	2.89
FM-Global-1 [16,19] [c]	12.1	63.7	5.40	C	295	0.17	0.01	3.96	366	0.70	2.48	1.71	1.00	1.69	1.26	2.18	1.52	0.10	1.01	1.00	7.14	241.84	11.77
FM-Global-2 [16,19] [c]	14.9	63.7	5.40	C	295	0.33	0.02	4.54	372	0.88	2.48	2.04	1.00	1.98	1.26	2.02	1.40	0.10	1.00	1.00	7.13	106.45	5.56
FM-Global-3 [16,19] [c]	16.5	63.7	5.40	C	295	0.46	0.03	4.86	375	0.99	2.48	2.23	1.00	2.13	1.26	1.93	1.35	0.10	1.00	1.00	7.04	71.19	3.90
FM-Global-4 [16,19] [c]	18	63.7	5.40	C	295	0.61	0.07	5.15	378	1.09	2.48	2.39	1.00	2.25	1.26	1.85	1.31	0.10	1.00	1.00	6.91	50.91	2.92
FM-Global-5 [16,19] [c]	18.1	63.7	5.40	C	295	0.62	0.06	5.16	378	1.10	2.48	2.40	1.00	2.26	1.26	1.85	1.31	0.10	1.00	1.00	6.90	49.86	2.87
FM-Global-6 [16,19] [c]	19	63.7	5.40	C	295	0.71	0.07	5.33	380	1.16	2.48	2.50	1.00	2.32	1.26	1.80	1.28	0.10	1.00	1.00	6.80	41.57	2.47
FM-Global-7 [16,19] [c]	19.1	63.7	5.40	C	295	0.73	0.11	5.35	381	1.17	2.48	2.51	1.00	2.33	1.26	1.80	1.28	0.10	1.00	1.00	6.79	40.77	2.43
FM-Global-8 [16,19] [c]	19.7	63.7	5.40	C	295	0.80	0.11	5.46	382	1.21	2.48	2.58	1.00	2.37	1.26	1.77	1.27	0.10	1.00	1.00	6.72	36.40	2.21
FM-Global-9 [16,19] [c]	17.5	63.7	2.70	C	295	0.56	0.23	5.05	377	1.06	2.48	2.34	1.00	2.21	1.26	1.88	1.32	0.10	1.00	1.00	6.95	28.34	1.60
FM-Global-10 [16,19] [c]	18	63.7	2.70	C	295	0.61	0.23	5.15	378	1.09	2.48	2.39	1.00	2.25	1.26	1.85	1.31	0.10	1.00	1.00	6.91	25.46	1.46
FM-Global-14 [16,19] [c]	16.5	63.7	5.40	R	295	0.46	0.09	4.86	375	0.99	2.48	2.23	1.00	2.13	1.26	1.93	1.35	0.10	1.00	1.00	7.04	71.19	3.90
FM-Global-15 [16,19] [c]	17.2	63.7	5.40	R	295	0.53	0.13	4.99	376	1.04	2.48	2.30	1.00	2.18	1.26	1.90	1.33	0.10	1.00	1.00	6.98	60.59	3.39
FM-Global-16 [16,19] [c]	17.9	63.7	5.40	R	295	0.60	0.15	5.13	378	1.09	2.48	2.38	1.00	2.24	1.26	1.86	1.31	0.10	1.00	1.00	6.92	52.00	2.97
FM-Global-17 [16,19] [c]	18.3	63.7	5.40	R	295	0.64	0.13	5.20	379	1.11	2.48	2.43	1.00	2.27	1.26	1.84	1.30	0.10	1.00	1.00	6.88	47.83	2.77
FM-Global-18 [16,19] [c]	19	63.7	5.40	R	295	0.71	0.19	5.33	380	1.16	2.48	2.50	1.00	2.32	1.26	1.80	1.28	0.10	1.00	1.00	6.80	41.57	2.47
FM-Global-19 [16,19] [c]	15.1	63.7	2.70	R	295	0.35	0.13	4.58	372	0.90	2.48	2.07	1.00	2.00	1.26	2.01	1.40	0.10	1.00	1.00	7.12	50.48	2.65
FM-Global-20 [16,19] [c]	17.1	63.7	2.70	R	295	0.52	0.25	4.97	376	1.03	2.48	2.29	1.00	2.18	1.26	1.90	1.33	0.10	1.00	1.00	6.99	30.98	1.73
FM-Global-21 [16,19] [c]	17.8	63.7	2.70	R	295	0.59	0.31	5.11	378	1.08	2.48	2.37	1.00	2.23	1.26	1.86	1.32	0.10	1.00	1.00	6.93	26.56	1.51
FM-Global-23 [16,19] [c]	18.2	63.7	5.40	F	295	0.63	0.04	5.18	379	1.11	2.48	2.42	1.00	2.26	1.26	1.84	1.30	0.10	1.00	1.00	6.89	48.83	2.82
FM-Global-24 [16,19] [c]	18	63.7	2.70	F	295	0.61	0.17	5.15	378	1.09	2.48	2.39	1.00	2.25	1.26	1.85	1.31	0.10	1.00	1.00	6.91	25.46	1.46
FM-Global-11 [16,19] [cd]	15.8	63.7	5.40	C	295	0.40	0.04	4.72	374	0.95	2.48	2.15	1.00	2.06	1.26	1.97	1.37	0.10	1.00	1.00	7.08	84.39	4.52
FM-Global-12 [16,19] [cd]	18.3	63.7	5.40	C	295	0.64	0.09	5.20	379	1.11	2.48	2.43	1.00	2.27	1.26	1.84	1.30	0.10	1.00	1.00	6.88	47.83	2.77
FM-Global-13 [16,19] [cd]	18.5	63.7	5.40	C	295	0.66	0.09	5.24	379	1.13	2.48	2.45	1.00	2.29	1.26	1.83	1.30	0.10	1.00	1.00	6.86	45.91	2.68
FM-Global-22 [16,19] [cd]	18.1	63.7	5.40	R	295	0.62	0.43	5.16	378	1.10	2.48	2.40	1.00	2.26	1.26	1.85	1.31	0.10	1.00	3.50	24.13	49.86	0.82
1P-H2 [21]	29.6	0.95	0.20	C	281	1.99	1.24	6.86	396	1.20	0.61	3.38	0.52	1.3	3.22	1.33	1	0	1	1	5.59	6.89	0.56
2P-H2 [21]	29.6	0.95	0.30	C	281	1.99	0.39	6.86	396	1.20	0.61	3.38	0.52	1.3	3.22	1.33	1	0	1	1	5.59	10.59	0.87

[a] C – central ignition; R – rear to vent ignition; N – near vent ignition. [b] S_{ui} – laminar burning velocity recalculated to account for initial temperature. [c] Reduced pressure for FM Global experiments are taken as a maximum of vibrational and "external deflagration" pressures. [d] Experiments with obstacles. [e] Ξ_{LP} and Ξ_{LP}^{max} are equal for chosen set of experiments, only one value is given.

*

*